

Study of charged Lepton Flavor Violation in electron muon interactions

Ran Ding,^a Jingshu Li,^a Meng Lu,^a Zhengyun You,^a Zijian Wang,^b and Qiang Li^b

^a*School of Physics, Sun Yat-Sen University, Guangzhou 510275, China*

^b*School of Physics and State Key Laboratory of Nuclear Physics and Technology, Peking University, Beijing, 100871, China*

E-mail: dingr25@mail2.sysu.edu.cn, lijsh53@mail2.sysu.edu.cn,
lumeng5@mail.sysu.edu.cn, youzhy5@mail.sysu.edu.cn,
wangzijian@stu.pku.edu.cn, qliphy0@pku.edu.cn

ABSTRACT: With the improvement of muon acceleration technology, it has received great interests to exploit high-energy muon beams for collision or target experiments. We investigate the possible charged Lepton Flavor Violation (cLFV) processes mediated by an extra massive neutral gauge boson Z' in electron muon interactions, either at a proposed electron muon collider or in a fixed target experiment with high-energy muon beam hitting electrons in the target. Based on Monte Carlo calculations and fast detector simulations, we study in detail the signal and possible backgrounds, giving the sensitivity results of cLFV signals at the 90% confidence level. Compared with the current and prospective limits set by other experiments, electron muon interactions demonstrate significant advantages in the cLFV coupling strength sensitivity with τ in the final states. In addition, a special cLFV coupling combination, $\lambda_{e\mu} \times \lambda_{\mu\mu}$, can also be probed in our proposal.

KEYWORDS: electron muon interaction, charged Lepton Flavor Violation, extra gauge boson

ARXIV EPRINT: [2405.09417](https://arxiv.org/abs/2405.09417)

Contents

1	Introduction	1
2	Physics processes and Monte Carlo simulation	3
2.1	cLFV in Z' model	3
2.2	Physics processes	3
2.3	Event generation and simulation	4
3	Statistical analysis and sensitivity result	5
3.1	Asymmetric collision	5
3.1.1	Background study	5
3.1.2	Sensitivity result	7
3.2	Electron-target experiment with a muon beam	9
4	Conclusion	12

1 Introduction

Collider experiment serves as a crucial tool for precision measurement of the standard model (SM) and search for new physics beyond the SM (BSM), with the experimental technology constantly being improved and evolved. In the near future, the High-Luminosity Large Hadron Collider (HL-LHC) [1], the Future Circular Collider (FCC) [2, 5, 6] or the Circular Electron Positron Collider (CEPC) [3, 4] may become important instruments for the next generation high energy frontier research. While recently with the continuous development of muon acceleration technology, the muon collider has also become an increasingly popular consideration. Since it integrates the advantages of electron colliders and hadron colliders, the muon collider may become a golden factory for studying various new physics processes [7].

On the other hand, high energy muon beams can also be used to create electron muon collisions. As early as ten to thirty years ago, numerous research efforts have already focused on the potential of electron muon collider [47–52]. In recent years, as the construction of high energy lepton collider gradually became feasible from the engineering standpoint, interest in electron-muon collision has been reignited [43–46].

Recently, a new collider proposal, μ TRISTAN, has been proposed based on an ultra-cold muon technology developed for the muon ($g - 2$) experiment at J-PARC [42]. It includes a $\mu^+\mu^+$ collider and a μ^+e^- collider, in which we are interested in the later. The main parameters from the μ TRISTAN $e\mu$ collider proposal [39, 42] are listed in Tab.1. According to several phenomenological study, μ TRISTAN may have certain potentials on measurements related to Higgs and new physics searches [38, 40, 41].

Table 1: The main parameters of the μ TRISTAN $e\mu$ collider.

Parameter	Electron	Anti-muon
Beam energy	30 GeV	1 TeV
Polarization	70%	>25%
Particles per bunch (10^{10})	6.2	1.4
Luminosity	$4.6 \times 10^{33} \text{ cm}^{-1}\text{s}^{-1}$	
Collision frequency	$4 \times 10^6 \text{ Hz}$	

Meanwhile, utilizing high-density muon beams to strike fixed targets can also provide a possibility to search for new physics. Many such attempts have been proposed, including the Muon Missing Momentum (M^3) proposal at Fermilab [55], and a recent idea of searching for muonic force carriers by using ATLAS detector as a fixed target [57].

In this study we also investigate a fixed electron-target experiment with a muon beam in addition to the $e\mu$ collider. As lepton flavor in the initial state is non-zero, electron muon interaction can strongly avoid many potential background processes which would occur at different-sign muon colliders or electron-positron colliders, thus possessing higher sensitivity to new physics signals, typically the charged Lepton Flavor Violation (cLFV) processes.

In the SM framework, the cLFV processes are strongly suppressed due to the tiny mass of neutrinos, hence unobservable in the current experiments yet. However, it may be much enhanced in various BSM models, such as super-symmetry (SUSY) [28], leptoquark [29], two-Higgs-doublet [36], R-parity-violating (RPV) Minimal Super-symmetric Standard Model (MSSM) [31–33], and the heavy neutral gauge boson Z' [30] studied in this paper. In the past decades, searches for the cLFV process were performed in different channels with several approaches, typically the high intensity muon-based experiments including $\mu^+ \rightarrow e^+\gamma$ (MEG) [12], $\mu^+ \rightarrow e^+e^+e^-$ (SINDRUM) [13] and $\mu^- N \rightarrow e^- N$ (SINDRUM II) [14–17], as well as the collider-based searches for cLFV decays of Z [18–20], Higgs [21, 22] and several hadron resonances [8–10, 23]. Meanwhile, there will be continuous new experiments conducted in the near future to constantly improve the existing limits, such as MEGII [24], Mu3e [25], COMET [27] and Mu2e [26].

In this study, we consider the cLFV processes based on the interactions of electron and muon in two scenarios: asymmetric electron muon collision at the $e\mu$ collider and fixed electron-target experiment striking with the muon beam. For the former case, the center-of-mass energy includes the energy point of μ TRISTAN and even higher. While for the latter case, we investigate the muon energy around several tens of GeV to test the Z' couplings at the low energy bound.

2 Physics processes and Monte Carlo simulation

2.1 cLFV in Z' model

By introducing an additional $U(1)$ gauge symmetry into the SM framework, it will correspond to a neutral gauge boson Z' . Since the heavy neutral gauge bosons are predicted in many BSM models, it may be one of the most motivated extensions of the SM [30, 34, 35].

In this study, we consider that there are not $Z - Z'$ mixing, and the extra Z' current has the same gauge coupling and chiral strength as the standard model Z^0 , but allows for the lepton flavor violation, similarly as Ref. [64, 67]. The coupling strength of the Z' and leptons can be described by a matrix λ as Eq. 2.1

$$\lambda = \begin{pmatrix} \lambda_{ee} & \lambda_{e\mu} & \lambda_{e\tau} \\ \lambda_{\mu e} & \lambda_{\mu\mu} & \lambda_{\mu\tau} \\ \lambda_{\tau e} & \lambda_{\tau\mu} & \lambda_{\tau\tau} \end{pmatrix}. \quad (2.1)$$

Generally, it represents the strength of the cLFV couplings relative to the SM couplings, assuming that the diagonal elements are 1, while the off-diagonal elements are usually a higher order of magnitude. Therefore, the cases that break lepton flavor conservation twice would not be considered in the further study. After introducing the Z' boson, the cLFV processes mentioned in Sec. 1 can be enhanced by the diagrams shown in Fig. 1. The branching ratio limits would be transformed to the coupling λ_{ij} [35] and compared with our results based on $e\mu$ interaction.

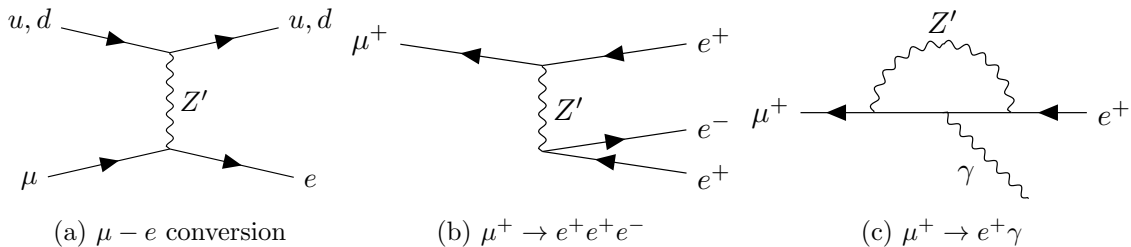


Figure 1: The Feynman diagrams of several Z' mediated cLFV processes.

2.2 Physics processes

The signal cLFV processes studied in this paper are listed in Tab. 2. There are two diagrams for the Z' mediated cLFV process $\mu^+e^- \rightarrow l^+l^-$, as shown in Fig. 2 (taking $\mu^+e^- \rightarrow e^+e^-$ as an example). In particular, the s-channel is not included in the processes $\mu^+e^- \rightarrow \mu^+\tau^-$. In the simulation, all coupling strengths are considered as 1. And the mass of Z' floats from 0.2 TeV to 5 TeV in the electron muon collision experiment, and within 0.50 GeV in the electron-target experiment with a muon beam.

While several background processes may occur on the collider and affect the signal that we are interested in, these processes include the standard model backgrounds divided by the number of final state particles and accidental background caused by particle mis-identification. Due to the suppression of phase space, we only consider the SM background

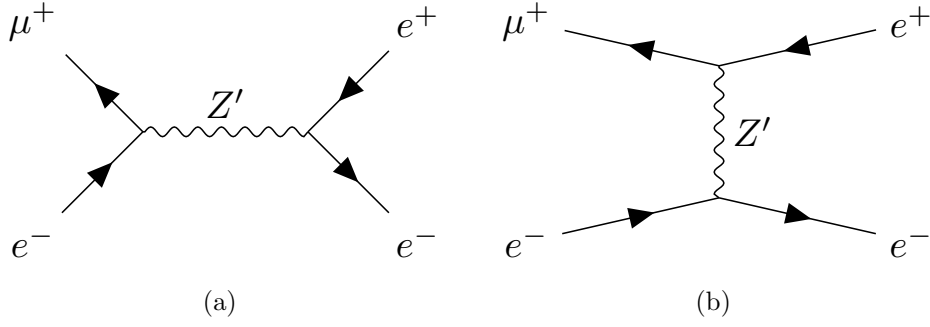


Figure 2: The Feynman diagrams of the process $\mu^+e^- \rightarrow e^+e^-$: (a) s-channel and (b) t-channel.

Table 2: Specific processes of signal and SM background

Signal Process	SM and accidental backgrounds.
$\mu^+e^- \rightarrow e^+e^-$	$\mu^+e^- \rightarrow e^+e^-\nu_e\bar{\nu}_\mu$ $\mu^+e^- \rightarrow e^+e^-\nu_e\bar{\nu}_\mu\nu\bar{\nu}$ $\mu^+e^- \rightarrow \mu^+e^-$
$\mu^+e^- \rightarrow \mu^+\mu^-$	$\mu^+e^- \rightarrow \mu^+\mu^-\nu_e\bar{\nu}_\mu$ $\mu^+e^- \rightarrow \mu^+\mu^-\nu_e\bar{\nu}_\mu\nu\bar{\nu}$ $\mu^+e^- \rightarrow \mu^+\mu^-$
$\mu^+e^- \rightarrow \mu^+\tau^-$	$\mu^+e^- \rightarrow \mu^+\tau^-\nu_e\bar{\nu}_\tau$ $\mu^+e^- \rightarrow \mu^+\tau^-\nu_e\bar{\nu}_\tau\nu\bar{\nu}$

with no more than 6 final state particles. In conclusion, the specific signals and their background processes are shown in Tab.2.

2.3 Event generation and simulation

Cross section and Monte Carlo events for each signal and background are calculated and simulated by MadGraph5_aMC@NLO(MG) [58] version 3.1.1, then showered and hadronized by Pythia8 [59]. Next, Delphes [60] version 3.5.1 is utilized to simulate detector effects with the default configuration card for the detector at the muon collider.

In the Monte Carlo generation, some preliminary requirements are applied to remove the physically unreasonable events. In $e\mu$ collisions, the transverse momentum of charged leptons is required to satisfy $p_T > 10$ GeV and the absolute pseudo-rapidity of charged leptons $|\eta| > 2.5$. While in the muon-beam electron-target simulation, the filtering criteria of p_T and $|\eta|$ would be relaxed. Then in the detector simulation, the parameters such as particle detection efficiency are set according to the default detector configuration in the Delphes cards.

There are some differences between the τ simulation and e/μ . For those final states with τ in Tab.2, although they can go through any decay chains in reality, in this study we

only consider the hadronic decay channels (about 60% of the total decay) and reconstruct it by the JET information.

3 Statistical analysis and sensitivity result

3.1 Asymmetric collision

In this scenario we consider two kinds of asymmetric collision with electron and anti-muon beam: $E_e = 30$ GeV and $E_\mu = 1$ TeV ($\sqrt{s} = 346$ GeV), or $E_e = 200$ GeV and $E_\mu = 3$ TeV ($\sqrt{s} = 1.55$ TeV). The former is based on the proposal of μ TRISTAN (the polarization of each beam is not considered), and the latter is a higher energy assumption according to other current beam designs.

3.1.1 Background study

Unlike e^+e^- or $\mu^+\mu^-$ collisions, since the initial lepton flavor in $e\mu$ collision is non-zero, vast majority of the SM backgrounds are forbidden, for example, $l^+l^- \rightarrow W^+W^-$ and $l^+l^- \rightarrow \tau^+\tau^-$. The typical diagrams for the SM background $\mu^+e^- \rightarrow l^+l^-\nu\bar{\nu}$ are shown in Fig.3.

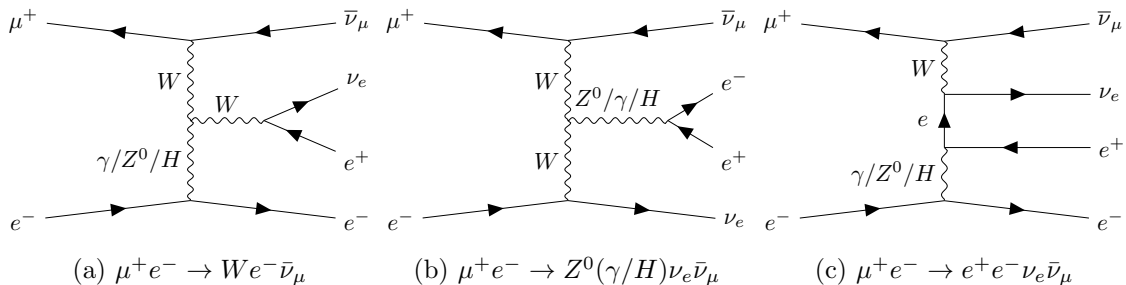


Figure 3: Typical diagrams for the SM background $\mu^+e^- \rightarrow l^+l^-\nu\bar{\nu}$, taking $\mu^+e^- \rightarrow e^+e^-\nu\bar{\nu}$ as an example. Especially, the diagram (b) does not appear in $\mu^+e^- \rightarrow \mu^+\tau^-\nu\bar{\nu}$.

After setting the preliminary requirements as mentioned in Sec.2.3, the signal candidate events should have the same charged leptons corresponding to the signal in the final state. According to the invariant mass distributions of the final state di-leptons as shown in Fig. 4, the remaining portion also exhibits significant kinematic differences from the signal processes, especially in $\mu^+e^- \rightarrow e^+e^-$ or $\mu^+e^- \rightarrow \mu^+\mu^-$ channel.

Only considering the interval near the center-of-mass energy, the SM background values are extremely low. And compared with a similar study on the different-signs electron or muon collider [64], $e\mu$ collision has a cleaner signal window. Due to the low level of the SM background, we also investigated the accidental background caused by $e\mu$ mis-identification, where a final state muon is mis-identified as an electron, or vice versa. Typically it would let the $e\mu$ scattering process coming into the background of $\mu^+e^- \rightarrow e^+e^-$ and $\mu^+e^- \rightarrow \mu^+\mu^-$. The probability of $e\mu$ mis-identification is set as 10^{-6} . The invariant mass distribution of this process is extremely close to the signal.

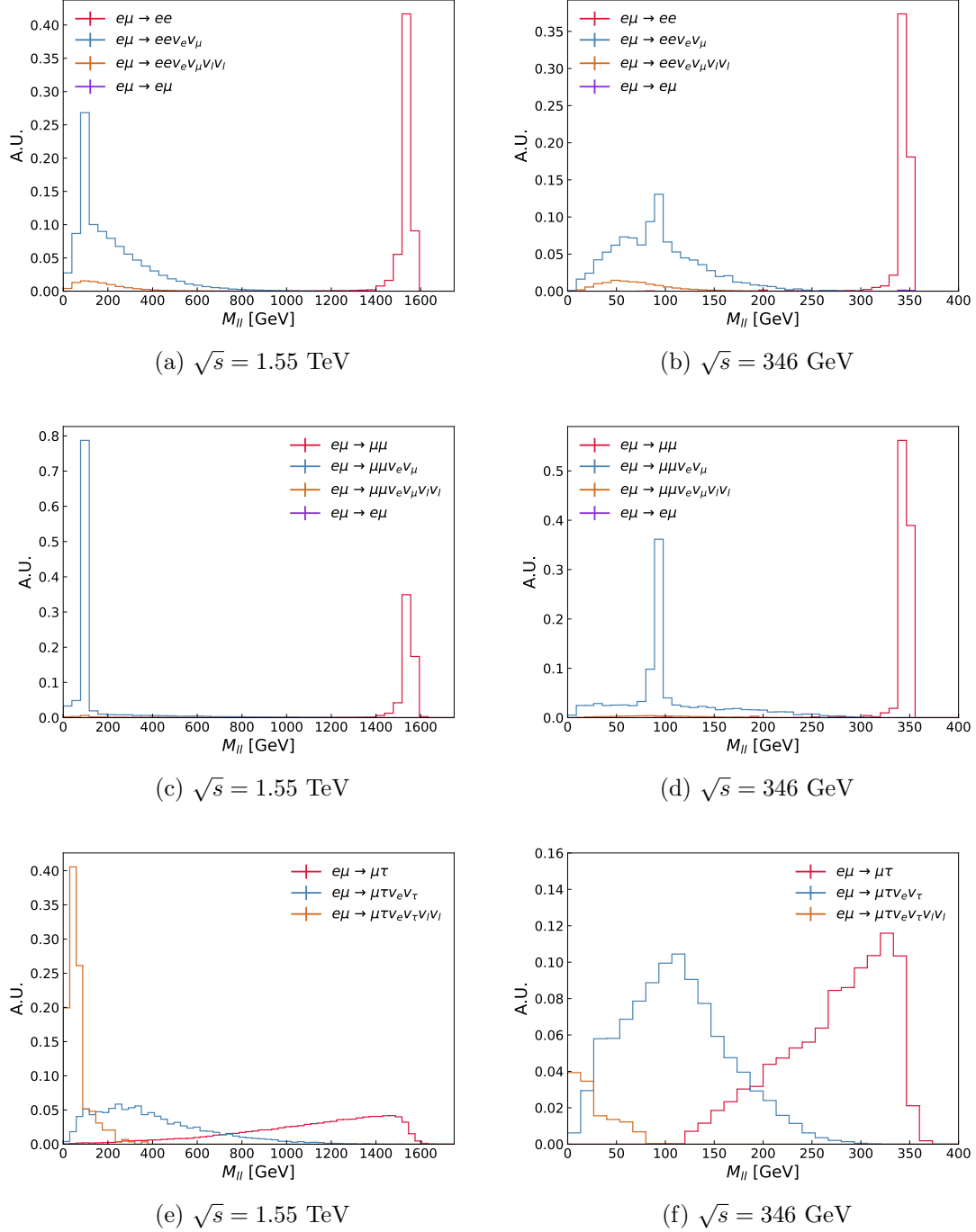


Figure 4: Distributions of the invariant mass reconstructed by the final state di-leptons, where the integral area of each background is determined by the cross section. Especially for the $e\mu$ scattering, it also includes the probability of particle mis-identification. Since the contribution of the background processes with six neutrinos is significantly lower than other kind of background, they will not be considered in the following analysis.

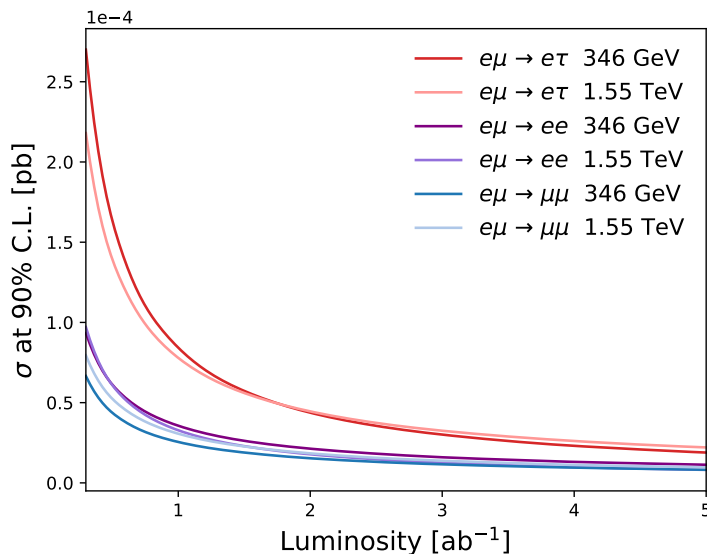


Figure 5: Cross section of each cLFV signal process of 90% C.L. exclusion relative to the luminosity of $e\mu$ collider.

While for $\mu^+e^- \rightarrow \mu^+\tau^-$, since the reconstruction of τ would inevitably result in a certain loss of energy, there is a considerable overlap in the signal and background distributions. The analysis will be optimized in the next section.

3.1.2 Sensitivity result

Based on the distributions of the signal and background as shown in Fig. 4, we truncate the invariant mass to remove the events with the reconstructed invariant mass significantly deviating from center-of-mass energy. For the cLFV channels without τ , the truncation points are set as 1.4 TeV for the 1.55 TeV collider, and 300 GeV for the μ TRISTAN. While in τ channels, it will be determined by scanning and selecting the maximum figure of merit (FOM) value of $S/(a/2 + \sqrt{B})$, where S is the number of signal events, B is the weighted number of the background $\mu^+e^- \rightarrow \mu^+\tau^-\nu_e\bar{\nu}_\tau$ and a is the significance value, which is usually set as 3 for new physics discoveries [65]. The weight for each process is defined by $n_x = \sigma_x L/N$, where σ_x is the cross section, L is the luminosity and N is the generated event number, which is 200,000 for each process. When $L = 0.3 \text{ ab}^{-1}$, the truncation point results are 1.27 TeV and 280 GeV for the two collider.

Then the binned histograms of leptons p_T distributions are utilized for the statistical analysis. The test statistics Z_i is calculated by $Z_i := 2[n_i - b_i + b_i \ln(n_i/b_i)]$ for 90% confidence level (C.L.) exclusion, where i is the index of each bin, n is the weighted number of observed events including signal and background, and b is the weighted number of background [66]. Then the total $Z = \sum_i Z_i$ would be subject to a χ^2 distribution. The degree of freedom is defined by the number of bins. By iteration, we can obtain the signal cross section of 90% C.L. exclusion, as shown in Fig. 5.

Table 3: Summary of the current and prospective limits from other experiments at 90% C.L.

Coupling	Channel	Constraint of branching ratio	
		Current	Prospective
$\lambda_{e\mu}$	$\mu N \rightarrow eN$	6.1×10^{-13} [17]	3.0×10^{-17} [27]
	$\mu \rightarrow eee$	1.0×10^{-13} [13]	1.0×10^{-16} [25]
	$\mu \rightarrow e\gamma$	4.2×10^{-13} [12]	6.0×10^{-14} [24]
$\lambda_{e\tau}$	$\tau \rightarrow e\gamma$	3.3×10^{-8} [11]	9.0×10^{-9} [68]
	$\tau \rightarrow \mu\mu e$	2.7×10^{-8} [11]	4.5×10^{-10} [68]
	$\tau \rightarrow eee$	2.7×10^{-8} [11]	4.7×10^{-10} [68]

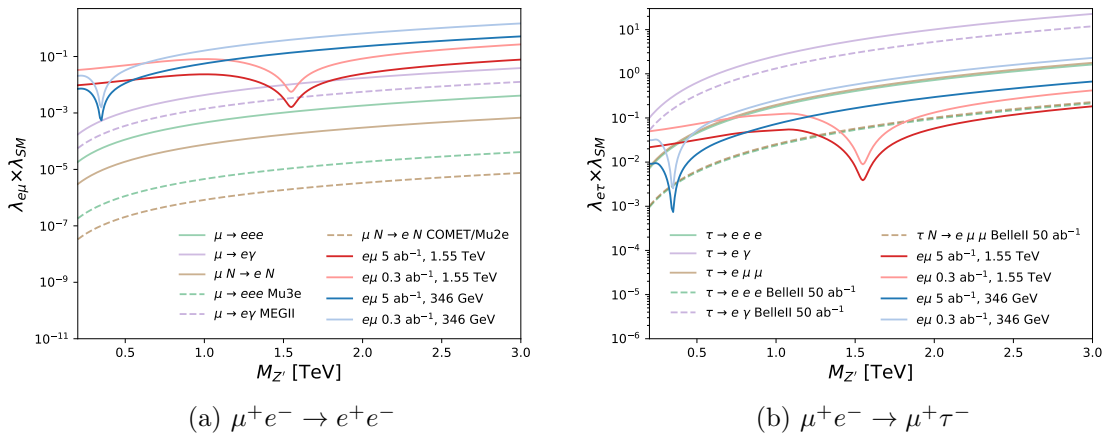


Figure 6: The 90% C.L. upper limit of $\lambda_{e\mu} \times \lambda_{SM}$ (a) and $\lambda_{e\tau} \times \lambda_{SM}$ (b). The curves are graphed with respect to $M_{Z'}$, representing the limits of the cross section times branching ratio. Additionally, exclusion lines from both present low-energy experiments (shown as solid lines in purple, green and brown) and future experiments (shown as dashed lines in purple, green and brown) are included in the plot.

Then based on MadGraph calculation we can get the corresponding value of $\lambda_{ij} \times \lambda_{SM}$, as shown in Fig. 6. Currently the coupling λ_{ij} are considered as positive real. Then the $\lambda_{e\mu}$ and $\lambda_{e\tau}$ results are calculated at two energy points, and the luminosity is 0.3 ab^{-1} or 5 ab^{-1} . Several current limits and prospective limits are also included to compare with our results. The constraints of branching ratio from other experiments are concluded in Tab. 3. It is sensible that the limits given by other experiments in τ channels are much more conservative than in $e\mu$ channels. But in our collider study, they may be similar since the main influencing factor here is the signal cross section while the cross sections of different signals are quite similar.

In the $\lambda_{e\mu}$ channel, the strictest constraint comes from the results of $\mu - e$ conver-

sion, and our results have weaker competitiveness among those high intensity muon-based experiments. While in the $\lambda_{e\tau}$ channel, current limits of $\tau \rightarrow eee$ and $\tau \rightarrow e\mu\mu$ perform the best across the entire interval, but the orders of magnitude are much lower than the results of $\lambda_{e\mu}$. Compared with our results, the constraints of 1.55 TeV $e\mu$ collider are more stringent than other existing results when $M_{Z'} > 0.5$ TeV, and for the 346 GeV collider it is about the entire $M_{Z'}$ interval. Even compared with the prospective limits of those processes on Belle II, our results still have certain advantages around the resonance region.

On the other side, comparing the results of $e\mu$ collision and e^+e^- or $\mu^+\mu^-$ collisions [64] based on the same luminosity, the results of $e\mu$ are better than $\mu^+\mu^-$ by an order of magnitude at their respective resonance points. But it cannot be ignored that the center-of-mass energy of $e\mu$ is relatively low, and the results of other experiments are more advantageous in the low-energy region. Furthermore, it is difficult for $e\mu$ collider to reach the same luminosity as that of $\mu^+\mu^-$ collider in reality. Therefore, the advantages of these two collision scenarios still need to be considered based on more practical factors.

To be precise, what we are comparing in Fig. 6a and Fig. 6b is the coupling $\lambda_{e\mu}(\lambda_{e\tau}) \times \lambda_{\text{SM}}$. Then based on the assumption that Z' has the same coupling structures and strengths as those of the standard model Z^0 mentioned in Sec. 2.1, which is $\lambda_{\text{SM}} = 1$, we can naturally obtain the estimation of $\lambda_{e\mu}$ or $\lambda_{e\tau}$. However, strictly speaking, this requirement may not exist in more universal models, and we need to consider the biases of standard model couplings. In this way, each process may give a product of different coupling strength, for example $\lambda_{e\mu} \times \lambda_{ee}$ ($\mu \rightarrow eee$) and $\lambda_{e\mu} \times \lambda_{ll}$ ($\mu \rightarrow e\gamma$), where l represents e or μ . Specially, we can obtain the measurement of the coupling $\lambda_{e\mu} \times \lambda_{\mu\mu}$ through $\mu^+e^- \rightarrow \mu^+\mu^-$ based on the $e\mu$ collider, as shown in Fig. 7, indicating that it has similar sensitivity as $\mu^+e^- \rightarrow e^+e^-$. While for the current high intensity experiments, this coupling only appears in $\mu \rightarrow e\gamma$ together with $\lambda_{e\mu} \times \lambda_{ee}$ according to Ref. [35], as

$$\Gamma(\mu \rightarrow e\gamma) = \frac{\alpha G_F^2 m_\mu^3 M_Z^4}{4\pi^4 M_{Z'}^4} \left[\sin^2 \theta_W \left(\sin^2 \theta_W - \frac{1}{2} \right) \right]^2 (\lambda_{ee}\lambda_{e\mu}m_e + \lambda_{e\mu}\lambda_{\mu\mu}m_\mu)^2, \quad (3.1)$$

where α is the fine structure constant, G_F is the fermi constant, θ_W is the weak mixing angle, M_Z , $M_{Z'}$, m_μ and m_e is the mass of Z^0 , Z' , μ and e , respectively.

Since the contribution of $\lambda_{e\mu} \times \lambda_{ee}$ is suppressed by the ratio of lepton masses, we can assume that this process is entirely composed of $\lambda_{e\mu} \times \lambda_{\mu\mu}$ and is comparable with our result as shown in Fig. 7. Meanwhile, if considering the rigorous contributions, it set the joint limitations on these two coupling strength, as shown in Fig. 8.

3.2 Electron-target experiment with a muon beam

Now we will focus on the low-energy region, where we conduct Monte Carlo simulations to investigate cLFV processes involving $\mu^+e^- \rightarrow e^+e^-$ and $\mu^+e^- \rightarrow \mu^+\mu^-$ in the electron-target experiment with a muon beam. It is essential to highlight that the masses of muon and electron cannot be disregarded, imposing a lower limit on the incident muon beam energy, equivalent to its mass. Additionally, the target experiment energy $E_{cm} = \sqrt{2E_\mu m_e + m_\mu^2 + m_e^2}$ possesses its own lower-energy threshold. Consequently, in our simulations, we vary the $M_{Z'}$ in three distinct sets for each process as shown in Tab. 4,

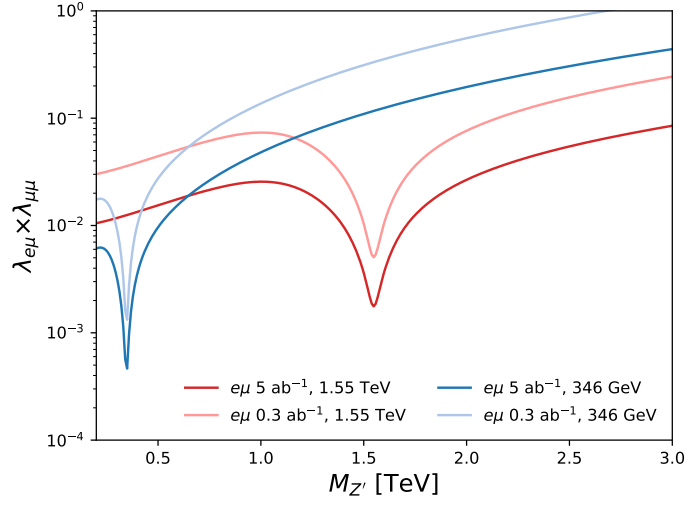


Figure 7: Sensitivity of the coupling strength $\lambda_{\mu\mu} \times \lambda_{e\mu}$ from $\mu^+e^- \rightarrow \mu^+\mu^-$ channel. Current and prospective results of $\mu \rightarrow e\gamma$ are include for comparison, assuming that it is entirely composed of $\lambda_{e\mu} \times \lambda_{\mu\mu}$.

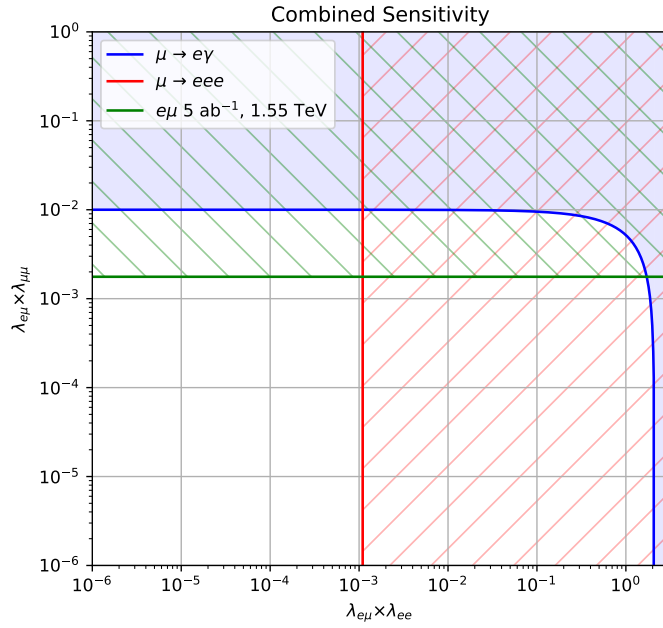


Figure 8: Sensitivity of the combined coupling strength at the resonance point of the 1.55 TeV $e\mu$ collider. The results of $\mu \rightarrow eee$ and $\mu \rightarrow e\gamma$ are calculated by the current limits. Each shaded area serves as the exclusion zone for the corresponding process.

Table 4: Resonant collision energy of process $\mu^+e^- \rightarrow e^+e^-$ and $\mu^+e^- \rightarrow \mu^+\mu^-$ with different $M_{Z'}$.

Process	$M_{Z'}$ / GeV	E_μ / GeV	E_e / MeV	E_{cm} / GeV
$\mu^+e^- \rightarrow e^+e^-$	0.11	0.93	0.511	0.1101
	0.15	11.1	0.511	0.1501
	0.20	28.2	0.511	0.1996
$\mu^+e^- \rightarrow \mu^+\mu^-$	0.22	33.6	0.511	0.2200
	0.25	50.2	0.511	0.2499
	0.30	77.2	0.511	0.2998

ensuring that the muon energy is scanned as close to the lower energy limit as feasible. The outcomes are shown in Fig. 9. Remarkably, a pronounced resonance in the target energy is observed in proximity to $M_{Z'}$.

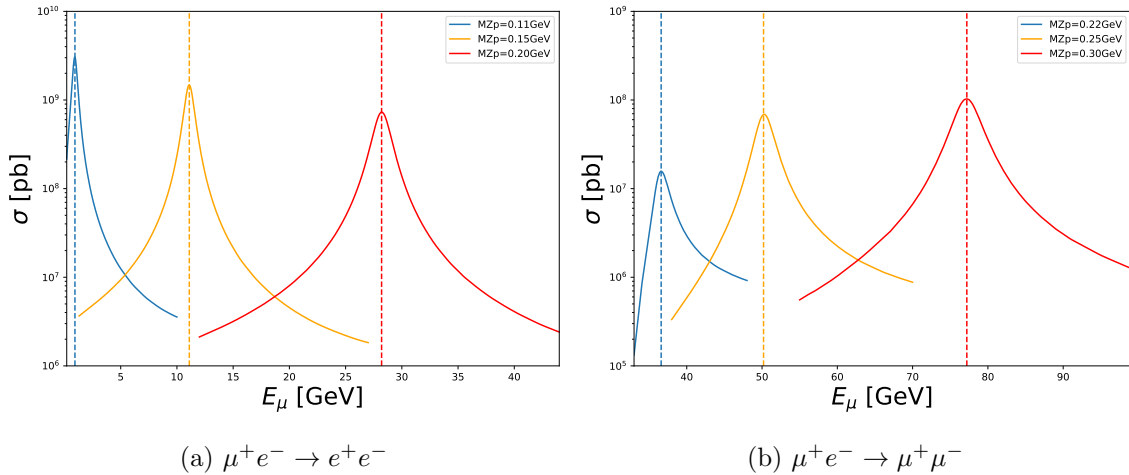


Figure 9: Cross section for resonant production of the process $\mu^+e^- \rightarrow e^+e^-$ and $\mu^+e^- \rightarrow \mu^+\mu^-$ with different $M_{Z'}$.

In this scenario, we conduct a background-free experimental estimation. Due to $\sigma \propto (\lambda_{e\mu} \times \lambda_{ll})^2$ and event rate $R = \frac{dN}{dt} \cdot n \cdot dx \cdot \sigma$, where $\frac{dN}{dt}$ denotes the muon production rate, n denotes the electron number density of the target material, dx denotes the thickness of the target, and σ denotes the reaction cross-section, coupling limits estimates can be made based on the reaction cross-section. As a rough estimate, assuming a 10 cm thick lead target, the incidence rate is about $\frac{dN}{dt} \sim 10^6 \text{s}^{-1}$, the electron number density of lead is about $n \sim 10^{24} \text{cm}^{-3}$, and $1\text{y} \sim 10^7 \text{s}$. From this estimation, we can obtain the 90% C.L. exclusion lines on the couplings λ_{ee} and $\lambda_{\mu\mu}$ products the diagonal coupling $\lambda_{e\mu}$.

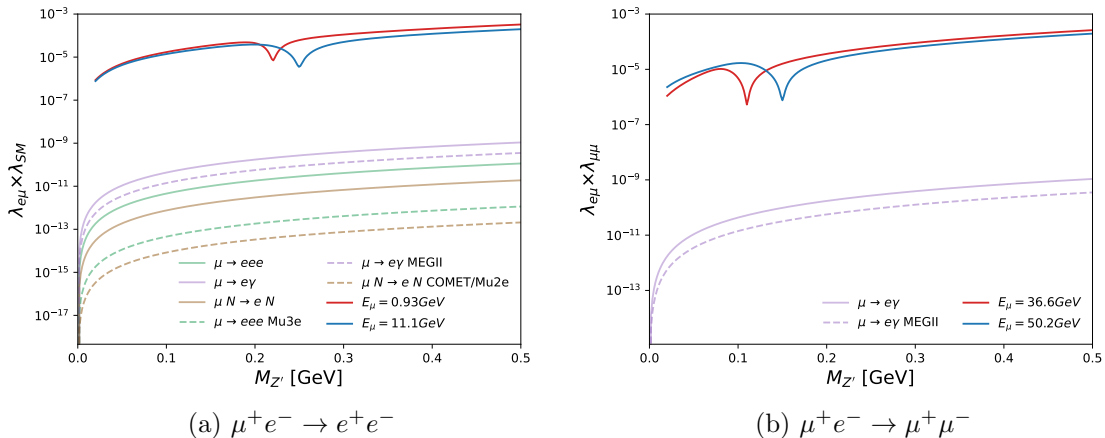


Figure 10: The 90% C.L. upper limit of $\lambda_{e\mu} \times \lambda_{SM}$ (a) and $\lambda_{e\mu} \times \lambda_{\mu\mu}$ (b). The curves are graphed with respect to $M_{Z'}$, representing the limits of the cross section times branching ratio. Additionally, exclusion lines from both present low-energy experiments (shown as solid lines in purple, green and brown) and future experiments (shown as dashed lines in purple, green and brown) are included in the plot.

Similarly, the current and prospective limits from low-energy experiments are converted to the coupling limits on $\lambda_{e\mu} \times \lambda_{SM}$ to compare with our results. As shown in Fig. 10a, compared with the existing experimental results and expected experimental results, the restrictions given here do not have obvious advantages. However, considering the $\mu\mu$ channel, if the coupling between Z' and $\mu\mu$ is much stronger than $e\mu$, that is, $\lambda_{e\mu} \ll \lambda_{\mu\mu}$, and assuming that the coupling strengths of other channels are all set to 0, then Z' decay mostly into $\mu\mu$, and the production cross section depends only on $\lambda_{e\mu}$. Accordingly, the resulted limit on $\lambda_{e\mu}$, compared with $\mu \rightarrow e\gamma$, can gain advantage of several orders of magnitudes. At the same time, if the data accumulation time of the muon beam experiment is considered to be 10 years, our estimated results will drop by another order of magnitude, which will improve the simulation results to a certain extent. However, it is worth noting that under the above estimation of the coupling strengths, $\Gamma_{Z'}$ will be reduced, which means that Z' will not be on resonance easily.

Additionally, since the result of $\mu \rightarrow e\gamma$ is related to the combination of $m_e\lambda_{e\mu}\lambda_{ee}$ and $m_\mu\lambda_{\mu\mu}\lambda_{e\mu}$ as Eq. 3.1, their inference may be non-ignorable. While our detection is exclusively sensitive to the $m_e\lambda_{e\mu}\lambda_{ee}$ term or the $m_\mu\lambda_{\mu\mu}\lambda_{e\mu}$ term, depending on the channel we choose.

4 Conclusion

With the continuous development of muon technology, in addition to building high-energy muon collider, there is also certain research prospect for the $e\mu$ interaction. In this work, we investigate the cLFV processes propagated by a massive neutral gauge boson (Z') in $e\mu$ collision and electron-target experiment with a muon beam, in order to explore the potential of $e\mu$ interactions in new physics searches. Using the MadGraph5_aMC@NLO,

Pythia8 and Delphes software, we conduct the simulation studies on the cLFV processes $\mu^+e^- \rightarrow e^+e^-$, $\mu^+e^- \rightarrow \mu^+\mu^-$ and $\mu^+e^- \rightarrow \mu^+\tau^-$. We then provide the coupling strength $\lambda_{e\mu}$ and $\lambda_{e\tau}$ at the 90% C.L. for different mass of Z' . By comparing the sensitivity results with the limits from the current and prospective experiments, it is shown that $e\mu$ interactions have certain research advantages in τ channel for the heavy Z' . Furthermore, based on the universal assumption, a unique process corresponding to coupling $\lambda_{e\mu} \times \lambda_{\mu\mu}$ can be measured, while this coupling combination can only appear in $\mu \rightarrow e\gamma$ channel among the current experiments.

Acknowledgments

This work is supported in part by the National Natural Science Foundation of China under Grant No. 12150005, 12075004, 12175321, 12061141003; the National Key Research and Development Program of China under Grant No. 2018YFA0403900; National College Students Innovation and Entrepreneurship Training Program, Sun Yat-sen University.

References

- [1] “High-Luminosity Large Hadron Collider (HL-LHC): Technical Design Report V. 0.1,” vol. 4/2017, 2017.
- [2] A. Abada *et al.*, “FCC Physics Opportunities: Future Circular Collider Conceptual Design Report Volume 1,” *Eur. Phys. J. C*, vol. 79, no. 6, p. 474, 2019.
- [3] “CEPC Conceptual Design Report: Volume 1 - Accelerator,” 9 2018.
- [4] M. Dong *et al.*, “CEPC Conceptual Design Report: Volume 2 - Physics & Detector,” 11 2018.
- [5] A. Abada *et al.*, “FCC-ee: The Lepton Collider: Future Circular Collider Conceptual Design Report Volume 2,” *Eur. Phys. J. ST*, vol. 228, no. 2, pp. 261–623, 2019.
- [6] —, “FCC-hh: The Hadron Collider: Future Circular Collider Conceptual Design Report Volume 3,” *Eur. Phys. J. ST*, vol. 228, no. 4, pp. 755–1107, 2019.
- [7] C. Aime *et al.*, “Muon Collider Physics Summary,” 3 2022.
- [8] E. Abouzaid *et al.*, “Search for lepton flavor violating decays of the neutral kaon,” *Phys. Rev. Lett.*, vol. 100, p. 131803, 2008.
- [9] W. Love *et al.*, “Search for Lepton Flavor Violation in Upsilon Decays,” *Phys. Rev. Lett.*, vol. 101, p. 201601, 2008.
- [10] J. P. Lees *et al.*, “Search for Lepton Flavor Violation in $\Upsilon(3S) \rightarrow e^\pm\mu^\mp$,” *Phys. Rev. Lett.*, vol. 128, no. 9, p. 091804, 2022.
- [11] K. Hayasaka *et al.*, “Search for Lepton Flavor Violating Tau Decays into Three Leptons with 719 Million Produced Tau+Tau- Pairs,” *Phys. Lett. B*, vol. 687, pp. 139–143, 2010.
- [12] A. M. Baldini *et al.*, “Search for the lepton flavour violating decay $\mu^+ \rightarrow e^+\gamma$ with the full dataset of the MEG experiment,” *Eur. Phys. J. C*, vol. 76, no. 8, p. 434, 2016.
- [13] U. Bellgardt *et al.*, “Search for the Decay $\mu^+ \rightarrow e^+e^+e^-$,” *Nucl. Phys. B*, vol. 299, pp. 1–6, 1988.

- [14] W. H. Bertl *et al.*, “A Search for muon to electron conversion in muonic gold,” *Eur. Phys. J. C*, vol. 47, pp. 337–346, 2006.
- [15] C. Dohmen *et al.*, “Test of lepton flavor conservation in $\mu \rightarrow e$ conversion on titanium,” *Phys. Lett. B*, vol. 317, pp. 631–636, 1993.
- [16] W. Honecker *et al.*, “Improved limit on the branching ratio of $\mu \rightarrow e$ conversion on lead,” *Phys. Rev. Lett.*, vol. 76, pp. 200–203, 1996.
- [17] J. Kaulard *et al.*, “Improved limit on the branching ratio of $\mu \rightarrow e$ conversion on titanium,” *Phys. Lett. B*, vol. 422, pp. 334–338, 1998.
- [18] G. Aad *et al.*, “Search for the lepton flavor violating decay $Z \rightarrow e\mu$ in pp collisions at \sqrt{s} TeV with the ATLAS detector,” *Phys. Rev. D*, vol. 90, no. 7, p. 072010, 2014.
- [19] R. Akers *et al.*, “A Search for lepton flavor violating Z^0 decays,” *Z. Phys. C*, vol. 67, pp. 555–564, 1995.
- [20] P. Abreu *et al.*, “Search for lepton flavor number violating Z^0 decays,” *Z. Phys. C*, vol. 73, pp. 243–251, 1997.
- [21] G. Aad *et al.*, “Searches for lepton-flavour-violating decays of the Higgs boson in $\sqrt{s} = 13$ TeV pp collisions with the ATLAS detector,” *Phys. Lett. B*, vol. 800, p. 135069, 2020.
- [22] A. M. Sirunyan *et al.*, “Search for lepton flavour violating decays of the Higgs boson to $\mu\tau$ and $e\tau$ in proton-proton collisions at $\sqrt{s} = 13$ TeV,” *JHEP*, vol. 06, p. 001, 2018.
- [23] M. Ablikim *et al.*, “Search for the lepton flavor violating decay $J/\psi \rightarrow e\mu$,” *Sci. China Phys. Mech. Astron.*, vol. 66, no. 2, p. 221011, 2023.
- [24] A. M. Baldini *et al.*, “The design of the MEG II experiment,” *Eur. Phys. J. C*, vol. 78, no. 5, p. 380, 2018.
- [25] K. Arndt *et al.*, “Technical design of the phase I Mu3e experiment,” *Nucl. Instrum. Meth. A*, vol. 1014, p. 165679, 2021.
- [26] L. Bartoszek *et al.*, “Mu2e Technical Design Report,” 10 2014.
- [27] R. Abramishvili *et al.*, “COMET Phase-I Technical Design Report,” *PTEP*, vol. 2020, no. 3, p. 033C01, 2020.
- [28] R. Barbier *et al.*, “R-parity violating supersymmetry,” *Phys. Rept.*, vol. 420, pp. 1–202, 2005.
- [29] I. Doršner, S. Fajfer, A. Greljo, J. F. Kamenik, and N. Košnik, “Physics of leptoquarks in precision experiments and at particle colliders,” *Phys. Rept.*, vol. 641, pp. 1–68, 2016.
- [30] P. Langacker, “The Physics of Heavy Z' Gauge Bosons,” *Rev. Mod. Phys.*, vol. 81, pp. 1199–1228, 2009.
- [31] D. Choudhury and P. Roy, “New constraints on lepton nonconserving R-parity violating couplings,” *Phys. Lett. B*, vol. 378, pp. 153–158, 1996.
- [32] M. Chemtob, “Phenomenological constraints on broken R parity symmetry in supersymmetry models,” *Prog. Part. Nucl. Phys.*, vol. 54, pp. 71–191, 2005.
- [33] X. Cai, J. Li, R. Ding, M. Lu, Z. You, and Q. Li, “Search for R-Parity-Violation-Induced Charged Lepton Flavor Violation at Future Lepton Colliders,” *Universe*, vol. 10, no. 6, p. 243, 3 2024.
- [34] A. J. Buras, A. Crivellin, F. Kirk, C. A. Manzari, and M. Montull, “Global analysis of leptophilic Z' bosons,” *JHEP*, vol. 06, p. 068, 2021.

- [35] P. Langacker and M. Plumacher, “Flavor changing effects in theories with a heavy Z' boson with family nonuniversal couplings,” *Phys. Rev. D*, vol. 62, p. 013006, 2000.
- [36] G. C. Branco, P. M. Ferreira, L. Lavoura, M. N. Rebelo, M. Sher, and J. P. Silva, “Theory and phenomenology of two-Higgs-doublet models,” *Phys. Rept.*, vol. 516, pp. 1–102, 2012.
- [37] J. Bernabeu, E. Nardi, and D. Tommasini, “ $\mu - e$ conversion in nuclei and Z' physics,” *Nucl. Phys. B*, vol. 409, pp. 69–86, 1993.
- [38] A. Das and Y. Orikasa, “ Z' induced forward dominant processes in μ TRISTAN experiment,” *Phys. Lett. B*, vol. 851, p. 138577, 2024.
- [39] D. Akturk, B. Dagli, and S. Sultansoy, “Muon Ring and FCC-ee / CEPC Based Antimuon-Electron Colliders,” 3 2024.
- [40] G. Lichtenstein, M. A. Schmidt, G. Valencia, and R. R. Volkas, “Complementarity of μ TRISTAN and Belle II in searches for charged-lepton flavour violation,” *Phys. Lett. B*, vol. 845, p. 138144, 2023.
- [41] Y. Hamada, R. Kitano, R. Matsudo, and H. Takaura, “Precision $\mu+\mu+$ and $\mu+e-$ elastic scatterings,” *PTEP*, vol. 2023, no. 1, p. 013B07, 2023.
- [42] Y. Hamada, R. Kitano, R. Matsudo, H. Takaura, and M. Yoshida, “ μ TRISTAN,” *PTEP*, vol. 2022, no. 5, p. 053B02, 2022.
- [43] A. O. Bouzas and F. Larios, “An electron-muon collider: what can be probed with it?” *Rev. Mex. Fis. Suppl.*, vol. 4, no. 2, p. 021128, 2023.
- [44] F. Bossi and P. Ciafaloni, “Lepton Flavor Violation at muon-electron colliders,” *JHEP*, vol. 10, p. 033, 2020.
- [45] M. Lu, A. M. Levin, C. Li, A. Agapitos, Q. Li, F. Meng, S. Qian, J. Xiao, and T. Yang, “The physics case for an electron-muon collider,” *Adv. High Energy Phys.*, vol. 2021, p. 6693618, 2021.
- [46] A. O. Bouzas and F. Larios, “Two-to-Two Processes at an Electron-Muon Collider,” *Adv. High Energy Phys.*, vol. 2022, p. 3603613, 2022.
- [47] V. D. Barger, S. Pakvasa, and X. Tata, “Are e mu colliders interesting?” *Phys. Lett. B*, vol. 415, pp. 200–204, 1997.
- [48] S. Y. Choi, C. S. Kim, Y. J. Kwon, and S.-H. Lee, “High-energy FCNC search through e mu colliders,” *Phys. Rev. D*, vol. 57, pp. 7023–7026, 1998.
- [49] J. C. Montero, V. Pleitez, and M. C. Rodriguez, “Left-right asymmetries in polarized e - mu scattering,” *Phys. Rev. D*, vol. 58, p. 097505, 1998.
- [50] G. Cvetič and C. S. Kim, “Heavy Majorana neutrino production at electron - muon colliders,” *Phys. Lett. B*, vol. 461, pp. 248–255, 1999, [Erratum: *Phys.Lett.B* 471, 471–472 (2000)].
- [51] F. M. L. Almeida, Jr., Y. do Amaral Coutinho, J. A. Martins Simoes, and M. A. B. Vale, do., “Single neutral heavy lepton production at electron muon colliders,” *Phys. Lett. B*, vol. 494, pp. 273–279, 2000.
- [52] J. K. Singhal, S. Singh, and A. K. Nagawat, “Possible exotic neutrino signature in electron muon collisions,” 3 2007.
- [53] A.-K. Perrevoort, “Charged lepton flavour violation - Overview of current experimental limits and future plans,” *PoS*, vol. DISCRETE2022, p. 015, 2024.

- [54] L. Calibbi and G. Signorelli, “Charged Lepton Flavour Violation: An Experimental and Theoretical Introduction,” *Riv. Nuovo Cim.*, vol. 41, no. 2, pp. 71–174, 2018.
- [55] Y. Kahn, G. Krnjaic, N. Tran, and A. Whitbeck, “ M^3 : a new muon missing momentum experiment to probe $(g - 2)$ and dark matter at Fermilab,” *JHEP*, vol. 09, p. 153, 2018.
- [56] J. Grange *et al.*, “Muon $(g-2)$ Technical Design Report,” 1 2015.
- [57] I. Galon, E. Kajamovitz, D. Shih, Y. Soreq, and S. Tarem, “Searching for muonic forces with the ATLAS detector,” *Phys. Rev. D*, vol. 101, no. 1, p. 011701, 2020.
- [58] J. Alwall, R. Frederix, S. Frixione, V. Hirschi, F. Maltoni, O. Mattelaer, H. S. Shao, T. Stelzer, P. Torrielli, and M. Zaro, “The automated computation of tree-level and next-to-leading order differential cross sections, and their matching to parton shower simulations,” *JHEP*, vol. 07, p. 079, 2014.
- [59] T. Sjöstrand, S. Ask, J. R. Christiansen, R. Corke, N. Desai, P. Ilten, S. Mrenna, S. Prestel, C. O. Rasmussen, and P. Z. Skands, “An introduction to PYTHIA 8.2,” *Comput. Phys. Commun.*, vol. 191, pp. 159–177, 2015.
- [60] J. de Favereau, C. Delaere, P. Demin, A. Giammanco, V. Lemaître, A. Mertens, and M. Selvaggi, “DELPHES 3, A modular framework for fast simulation of a generic collider experiment,” *JHEP*, vol. 02, p. 057, 2014.
- [61] G. D. Maso *et al.*, “Future facilities at PSI, the High-Intensity Muon Beams (HIMB) project,” *EPJ Web Conf.*, vol. 282, p. 01012, 2023.
- [62] M. Bogomilov *et al.*, “Transverse Emittance Reduction in Muon Beams by Ionization Cooling,” 10 2023.
- [63] —, “Demonstration of cooling by the Muon Ionization Cooling Experiment,” *Nature*, vol. 578, no. 7793, pp. 53–59, 2020.
- [64] J. Li, W. Wang, X. Cai, C. Yang, M. Lu, Z. You, S. Qian, and Q. Li, “A Comparative Study of Z' mediated Charged Lepton Flavor Violation at future lepton colliders,” *JHEP*, vol. 03, p. 190, 2023.
- [65] G. Punzi, “Sensitivity of searches for new signals and its optimization,” *eConf*, vol. C030908, p. MODT002, 2003.
- [66] G. Cowan, K. Cranmer, E. Gross, and O. Vitells, “Asymptotic formulae for likelihood-based tests of new physics,” *Eur. Phys. J. C*, vol. 71, p. 1554, 2011, [Erratum: *Eur.Phys.J.C* 73, 2501 (2013)].
- [67] M. Aaboud *et al.*, “Search for lepton-flavor violation in different-flavor, high-mass final states in pp collisions at $\sqrt{s} = 13$ TeV with the ATLAS detector,” *Phys. Rev. D*, vol. 98, no. 9, p. 092008, 2018.
- [68] S. Banerjee, “Searches for Lepton Flavor Violation in Tau Decays at Belle II,” *Universe*, vol. 8, no. 9, p. 480, 2022.